

This document is confidential and is proprietary to the American Chemical Society and its authors. Do not copy or disclose without written permission. If you have received this item in error, notify the sender and delete all copies.

Ion Mobility-Mass Spectrometry of Iodine Pentoxide-Iodic Acid Hybrid Cluster Anions in Dry and Humidified Atmosphere

Journal:	<i>The Journal of Physical Chemistry Letters</i>
Manuscript ID	jz-2019-00453d.R1
Manuscript Type:	Letter
Date Submitted by the Author:	n/a
Complete List of Authors:	Ahonen, Lauri; University of Helsinki, Institute for Atmospheric and Earth System Research (INAR) Li, Chenxi; ETH, Dep. of Chemistry and Applied Biosc.; University of Minnesota Twin Cities, Mechanical Engineering Kubecka, Jakob; University of Helsinki, Institute for Atmospheric and Earth System Research (INAR) Iyer, Siddharth; Helsingin Yliopisto, Department of molecular sciences Vehkamäki, Hanna; Helsingin Yliopisto, Department of Physical Sciences Petäjä, Tuukka; Helsingin Yliopisto, Kulmala, Markku; Helsingin Yliopisto, Dept. of Physical Sciences Hogan, Christopher; University of Minnesota Twin Cities, Mechanical Engineering

SCHOLARONE™
Manuscripts

1
2
3
4
5
6
7
8
9
10
11
12
13
14
15
16
17
18
19
20
21
22
23
24
25
26
27
28
29
30
31
32
33
34
35
36
37
38
39
40
41
42
43
44
45
46
47
48
49
50
51
52
53
54
55
56
57
58
59
60

Ion Mobility-Mass Spectrometry of Iodine Pentoxide-Iodic Acid Hybrid Cluster Anions in Dry and Humidified Atmosphere

*Lauri Ahonen¹, Chenxi Li^{2,3}, Jakub Kubečka¹, Siddharth Iyer⁴, Hanna Vehkamäki¹, Tuukka
Petäjä¹, Markku Kulmala¹ and Christopher. J. Hogan Jr.^{2*}*

¹Institute for Atmospheric and Earth System Research/Physics, Faculty of Science, University of
Helsinki, 00014 Helsinki, Finland.

²Department of Mechanical Engineering, University of Minnesota, Minneapolis, MN 55455,
USA

³Laboratory for Physical Chemistry, ETH Zürich, 8093 Zürich, Switzerland

⁴Institute for Atmospheric and Earth System Research/Chemistry, University of Helsinki, P.O.
Box 55, FI-00014 Helsinki, Finland

AUTHOR INFORMATION

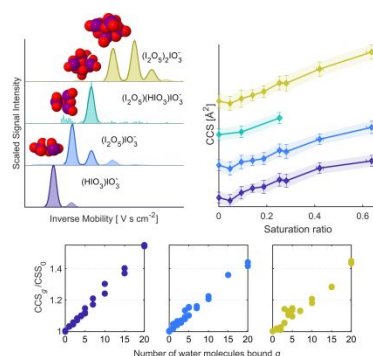
Corresponding Author

*To whom correspondence should be addressed: hogan108@umn.edu, T: 1-612-626-8312

ABSTRACT

Nanometer scale clusters form from vapor phase precursors and can subsequently grow into nanoparticles during atmospheric nucleation events. A particularly interesting set of clusters relevant to nucleation is hybrid iodine pentoxide-iodic acid clusters of the form $(\text{I}_2\text{O}_5)_x(\text{HIO}_3)_y$, as these clusters have been observed in coastal region nucleation events in anomalously high concentrations. To better understand their properties, we have utilized ion mobility-mass spectrometry to probe the structures of cluster anions of the form $(\text{I}_2\text{O}_5)_x(\text{HIO}_3)_y(\text{IO}_\alpha)^-$ ($x = 0 - 7$, $y = 0 - 1$, $\alpha = 1 - 3$), similar to those observed in coastal nucleation events. We show that $(\text{I}_2\text{O}_5)_x(\text{HIO}_3)_y(\text{IO}_\alpha)^-$ clusters are relatively stable against dissociation during mass spectrometric measurement, as compared to other clusters observed in nucleation events over continental sites, and that at atmospherically relevant relative humidity levels (65% and less), clusters can become sufficiently hydrated to facilitate complete conversion of iodine pentoxide to iodic acid, but that water sorption beyond this level is limited, indicating that the clusters do not persist as nanometer scale droplets in the ambient.

TOC GRAPHIC



1
2
3 Atmospheric nucleation events occur when vapor phase precursors bind to one another,
4 forming stable, condensed phase molecular clusters.¹⁻³ Though considerable progress has been
5 made in understanding atmospheric nucleation via a combination of field measurements,
6 laboratory experiments, and computational models,⁴⁻¹¹ prediction of nucleation rates and
7 construction of accurate cluster to nanoparticle growth models both remain difficult. This is in
8 large part because the physicochemical properties of nucleation event formed clusters, which
9 determine both their stability and their potential for subsequent growth, have not been fully
10 characterized. Limitations in signal intensity and in cluster lifetime in the ambient typically
11 prohibit in-situ characterization beyond chemical identification.
12
13
14
15
16
17
18
19
20
21
22
23

24 There is therefore interest in greater characterization of the stability, structure, and
25 hydration (as clusters in the ambient are in frequent contact with water) of clusters identified as
26 forming during atmospheric nucleation events. A particularly pertinent, yet relatively unstudied
27 class of clusters are iodine pentoxide-iodic acid hybrid clusters of the form $(\text{I}_2\text{O}_5)_x(\text{HIO}_3)_y$.
28 These clusters have been observed to form from biogenic iodine precursors during nucleation
29 events in coastal regions,¹²⁻¹⁶ wherein the cluster formation and growth rates are anomalously
30 high¹⁷ in comparison to continental nucleation events. In this study, we have utilized ion
31 mobility-mass spectrometry (IM-MS,¹⁸ with a high resolution differential mobility analyzer
32 coupled to a mass spectrometer¹⁹) to measure the collision cross sections (CCSs) of cluster
33 anions of the form $(\text{I}_2\text{O}_5)_x(\text{HIO}_3)_y(\text{IO}_\alpha)^-$ with $x = 0 - 7$, $y = 0 - 1$, and $\alpha = 1 - 3$. In using IM-
34 MS as a cluster characterization technique, we follow the methods outlined by Oberreit *et al*²⁰
35 and Thomas *et al*,²¹ with three specific objectives: (1) we assess relative cluster ion stability by
36 monitoring dissociation between atmospheric pressure mobility measurements and low pressure
37 mass spectrometry measurements; (2) we compare the CCSs, which were measured in CO_2 , to
38
39
40
41
42
43
44
45
46
47
48
49
50
51
52
53
54
55
56
57
58
59
60

1
2
3 CCS predictions based on both specular and diffuse gas molecule scattering predictions with all-
4 atom cluster models;²²⁻²³ and (3) we examine CCS shifts in the presence of water vapor (near 295
5 K, at saturation ratios of up to 0.65).
6
7
8
9

10 Differential mobility analysis-mass spectrometer measurements were performed on
11 electrospray generated cluster anions (using 1 mM iodic acid in HPLC water), with additional
12 details on measurements provided in the *Supporting Information*. In using electrospray
13 ionization to generate clusters, we assume that the clusters formed, for a given chemical
14 composition, adopt similar structures to those generated during atmospheric nucleation, i.e.
15 clusters “equilibrate” to conformations which are not dependent on their formation process.
16 Measurements result in detected ion signal as a function of mass-to-charge ratio and the applied
17 differential mobility analyzer voltage, which is convertible to inverse mobility after
18 instrumentation calibration.²⁴⁻²⁵ Contour plots of raw data for cluster ions with mobility
19 measurements made in dry CO₂ at 295 K (with immeasurably low water content, below 1%
20 relative humidity) are shown in Figure 1a. Signal corresponding to ions of a specific composition
21 and specific structure take the form of “line segments”, and line segments are grouped by charge-
22 state. We focus solely on the singly charged cluster ions in this study, as multiply charged
23 clusters are generally unique to electrospray ionization and are unlikely to be observed in
24 atmospheric nucleation events. For selected singly charged cluster ions where the excess charge
25 is carried by the IO₃⁻ ion, post-calibration inverse mobility spectra are provided in Figure 1b.
26 Evident in the figure, for all ions, there are multiple peaks detected. In many instances, peaks of
27 “neighboring” cluster ions, i.e. cluster ions with compositions differing by a single iodine
28 pentoxide (I₂O₅) or iodic acid (HIO₃), or with I₂O₅ displaced by HIO₃, coincide exactly with one
29 another in location. In IM-MS measurements this is known to arise because of either
30
31
32
33
34
35
36
37
38
39
40
41
42
43
44
45
46
47
48
49
50
51
52
53
54
55
56
57
58
59
60

dissociation reactions (*i.e.* $(\text{I}_2\text{O}_5)_x(\text{HIO}_3)_y(\text{IO}_3)^- \rightarrow (\text{I}_2\text{O}_5)_{x-1}(\text{HIO}_3)_y(\text{IO}_3)^- + \text{I}_2\text{O}_5$ and $(\text{I}_2\text{O}_5)_x(\text{HIO}_3)(\text{IO}_3)^- \rightarrow (\text{I}_2\text{O}_5)_x(\text{IO}_3)^- + \text{HIO}_3$) or displacement reactions (the reaction $(\text{I}_2\text{O}_5)_x(\text{IO}_3)^- + \text{H}_2\text{O} \rightarrow (\text{I}_2\text{O}_5)_{x-1}(\text{HIO}_3)(\text{IO}_3)^- + \text{HIO}_3$ in this instance) after mobility measurement but prior to mass measurement.²⁶ Signal appears in such instances at the inverse mobility of the parent ion, but the mass-to-charge ratio of the product ion. For all detected clusters ions, the peaks of the smallest inverse mobilities can be identified as arising from unreacted parent ions. However, for all cluster ions smaller than $(\text{I}_2\text{O}_5)_4\text{IO}_3^-$, the secondary and tertiary peaks at higher inverse mobilities clearly align with peaks in the inverse mobility spectra of higher mass ions; this suggests that they arise from dissociation or displacement reactions. For $(\text{I}_2\text{O}_5)_x\text{IO}_3^-$ with $x = 4 - 7$ (with the spectrum for $x = 7$ not shown), secondary inverse mobility peaks are apparent, yet these peaks do not coincide with peaks in the spectra of larger ions. They are likely indicative of a second, unique structure type adopted by larger cluster ions which does not interconvert with the lower inverse mobility structure type during measurement.

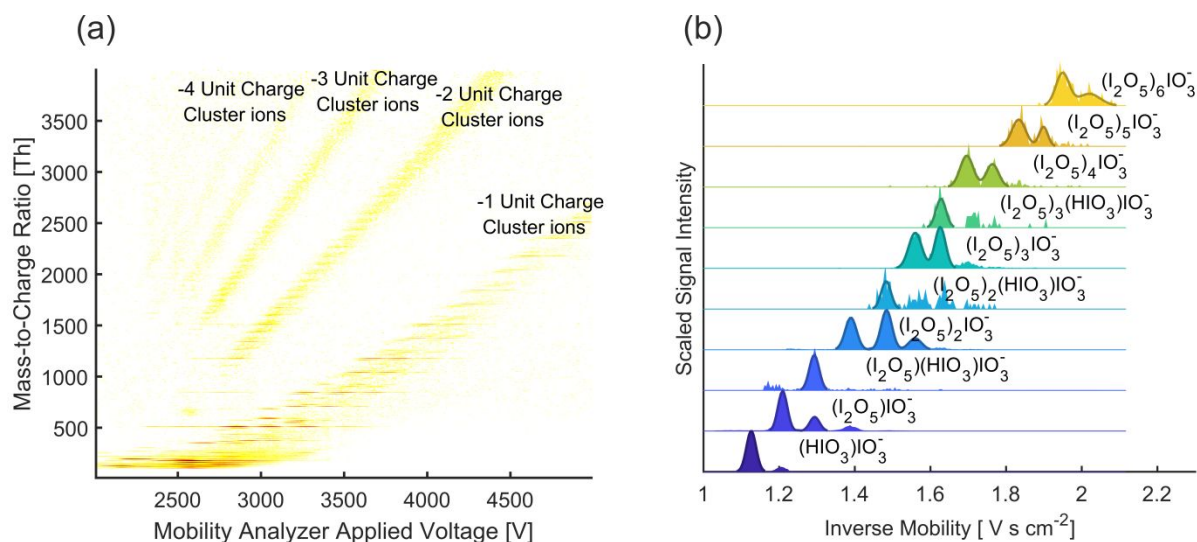


Figure 1. (a) A contour plot of measured signal intensity as a function of mass-to-charge ratio and mobility analyzer applied voltage for electrospray generated cluster anions. (b) Post-calibration inverse mobility spectra for specific mass identified cluster anions. The chemical compositions of the selected ions are noted.

1
2
3 The differential mobility analyzer-mass spectrometer system employed has been utilized
4 under identical measurement conditions (including inlet voltage settings) to analyze a variety of
5 other cluster ions. The extent of dissociation reactions observed here can be compared to these
6 prior results, and hence used to qualitatively assess the stability of hybrid iodine pentoxide-iodic
7 acid cluster ions. Ouyang *et al.*²⁷ examined positively charged alkali metal-iodide cluster ions of
8 the form $(\text{XI})_n\text{X}^+$ ($\text{X} = \text{Na}, \text{K}, \text{Rb}, \text{Cs}$ and $n = 1-13$), and Thomas *et al.*²¹ examined positively and
9 negatively charged hybrid dimethylammonium bisulfate-sulfuric acid cluster ions with up to 8
10 dimethylammonium bisulfate ion-pairs and 3 sulfuric acid molecules (which are similar in
11 composition to those detected in atmospheric nucleation events in a number of continental
12 sites).^{5-7, 28-29} In both of these prior studies, multiple successive dissociation reactions were
13 observed to take place subsequent to mobility analysis and prior to mass analysis; for positively
14 charged dimethylammonium bisulfate-sulfuric acid cluster ions dissociation was often severe
15 enough to leave parent ions undetectable. The extent of dissociation and displacement reaction
16 observed in this study is much less for iodine pentoxide-iodic acid hybrid clusters than observed
17 in prior studies of other cluster ion types. They can thus be regarded as a particularly stable class
18 of cluster anions compared to those studied previous via atmospheric pressure IM-MS. We
19 postulate that their high levels of stability may contribute to the high nucleation rates observed
20 when such clusters form, as when dissociation is minimal, the nucleation rate can approach a
21 collision-controlled limit.³⁰⁻³¹

22
23
24
25
26
27
28
29
30
31
32
33
34
35
36
37
38
39
40
41
42
43
44
45
46
47 More direct than stability, IM-MS measurements yield the CCSs of the identified cluster
48 ions via application of the Mason-Schamp equation (the equation linking mobility/diffusivity to
49 collision cross section).³² By comparing measurement results to predictions of CCSs based on
50 computationally derived structures, we can assess to what extent computationally modelled
51
52
53
54
55
56
57
58
59
60

1
2
3 structures capture the global structural features of clusters. In the experiment-model comparison
4 we considered only the CCSs of ions based upon the primary peak (lowest inverse mobility) in
5 each inverse mobility spectrum, as we are confident these peaks do not arise from post-mobility
6 analyzer dissociation or displacement reactions. Experimentally inferred CCSs for these ions are
7 noted in Table 1. Candidate cluster structures for CCS calculations were generated as described
8 in the *Supporting Information*. Briefly, for the clusters $(\text{HIO}_3)\text{IO}_3^-$, $(\text{I}_2\text{O}_5)\text{IO}_3^-$ and
9 $(\text{I}_2\text{O}_5)(\text{HIO}_3)\text{IO}_3^-$, structures were optimized using Density Functional Theory (DFT) at the
10 $\omega\text{B97xD//aug-cc-pVTZ-PP}$ level. For larger clusters, cluster structures were identified by first
11 determining the partial atomic charges extracted for each of the iodine-containing monomer
12 acids, oxides, and anions (i.e. HIO_3 , I_2O_5 , and IO_3^-) in cluster ions by running a single-point
13 population analysis calculation, and then using partial charges in configurational sampling via
14 the Artificial Bee Colony (ABC) algorithm³³ with rigid molecules to construct clusters, which
15 were again reoptimized with a low DFT level of theory. To compute CCSs, we utilized IMoS,²²⁻
16 ²³ considering the ion-induced dipole potential between impinging CO_2 molecules and clusters,³⁴⁻
17 ³⁵ but treating atoms as hard spheres, considering both elastic hard sphere scattering (EHSS) and
18 diffuse hard sphere scattering (DHSS) models. In the EHSS model, gas molecule collisions are
19 modeled as elastic and specular (translational kinetic energy is conserved), while in the DHSS
20 model, gas molecules are reemitted from the ion surface at a diffuse angle (randomly selected)
21 upon impingement on the ion surface, and the gas molecule's velocity is resampled from a
22 modified Maxwell-Boltzmann distribution.²² Discussed previously,^{27, 36} for nanometer scale ions
23 these two scattering models lead to appreciable differences in CCS predictions (as much as 30%
24 in many instances), and for polyatomic gas molecules such as CO_2 , we expect that the DHSS
25
26
27
28
29
30
31
32
33
34
35
36
37
38
39
40
41
42
43
44
45
46
47
48
49
50
51
52
53
54
55
56
57
58
59
60

model should more accurately describe gas molecule scattering process on an ion modeled as frozen (fixed) during calculation.^{27, 35-37}

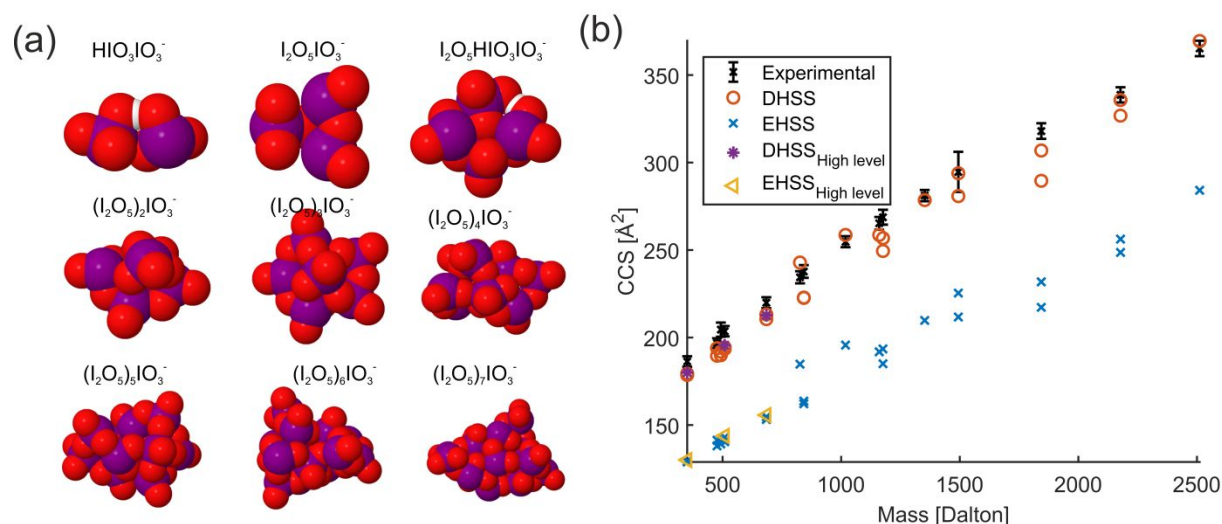


Figure 2. (a) Depictions of selected cluster ion candidate structures. Purple: Iodine atoms. Red: Oxygen Atoms. (b) Experimentally inferred and calculated CCSs as a function of cluster ion mass. The subscript “High Level” refers to structures obtained from density function theory (ω B97xD//aug-cc-pVTZ-PP level) using a sufficiently large basis set. Error bars are based upon the uncertainty in the mobility analyzer voltage corresponding to the peak signal intensity.

Table 1. A summary of the cluster formulae, masses, measured CCSs, and predicted CCSs using the EHSS and DHSS calculation approaches. N is the number of candidate cluster structures, with the predicted CCSs shown for each candidate.

Molecular formula	mass [Da]	CCS [\AA^2]	N	EHSS [\AA^2]		DHSS [\AA^2]	
$(\text{HIO}_3)_1\text{IO}_2^-$	334	187 ± 4	0				
$(\text{HIO}_3)_1\text{IO}_3^-$	350	186 ± 3	2	129	129	179	179
$(\text{I}_2\text{O}_5)_1\text{IO}^-$	476	197 ± 3	2	138	141	190	194
$(\text{I}_2\text{O}_5)_1\text{IO}_2^-$	492	205 ± 4	2	139	141	190	192
$(\text{I}_2\text{O}_5)_1\text{IO}_3^-$	508	204 ± 3	2	140	143	193	194
$(\text{HIO}_3)_2\text{IO}_2^-$	510	203 ± 3	0				
$(\text{I}_2\text{O}_5)_1(\text{HIO}_3)\text{IO}_3^-$	684	220 ± 3	2	153	155	211	213
$(\text{I}_2\text{O}_5)_2\text{IO}_2^-$	826	234 ± 3	1	185		243	
$(\text{I}_2\text{O}_5)_2\text{IO}_3^-$	842	238 ± 4	1	164	162	223	223
$(\text{I}_2\text{O}_5)_2(\text{HIO}_3)\text{IO}_3^-$	1018	255 ± 3	1	196		259	

$(\text{I}_2\text{O}_5)_3\text{IO}_2^-$	1160	265 ± 4	1	192		259	
$(\text{I}_2\text{O}_5)_3\text{IO}_3^-$	1176	269 ± 4	2	185	194	249	257
$(\text{I}_2\text{O}_5)_3(\text{HIO}_3)\text{IO}_3^-$	1352	281 ± 3	1	210		279	
$(\text{I}_2\text{O}_5)_4\text{IO}_2^-$	1494	295 ± 11	0				
$(\text{I}_2\text{O}_5)_4\text{IO}_3^-$	1510	293 ± 4	2	225	212	294	281
$(\text{I}_2\text{O}_5)_3(\text{HIO}_3)_3\text{IO}_3^-$	1703	314 ± 6	0				
$(\text{I}_2\text{O}_5)_5\text{IO}_3^-$	1843	318 ± 4	2	232	217	307	290
$(\text{I}_2\text{O}_5)_6\text{IO}_3^-$	2177	339 ± 4	2	249	256	327	336
$(\text{I}_2\text{O}_5)_7\text{IO}_3^-$	2511	365 ± 4	1	284		369	

Predicted CCSs based on the two models are shown in Table 1 for direct comparison to experimentally inferred values. Depictions of the cluster ion structures employed in calculations (for selected clusters) are shown in Figure 2a, and a plot of measurement inferred and calculated CCSs as a function of cluster ion mass is shown in Figure 2b. Calculation results are shown for multiple potential cluster ion structures. Consistent with prior studies on the influence of cluster structure on the CCS,³⁸ differences in the predicted CCSs for different structures are significantly smaller than the influence of scattering model. Results show clearly that DHSS model predictions are in good agreement with measurements. Noteworthy about this is that neither candidate structure characterization nor CCS calculations utilized input parameters which were “fit” to measurements, and it demonstrates that both the higher level and lower level computations of cluster ion structures accurately capture global structure features of clusters.

Prior work has shown that by adding condensable vapor in mobility analyzers, the sorption/binding of vapor can be examined at the molecular level, as binding, even transiently, leads to detectible mobility/CCS shifts.^{20, 39-40} For iodine pentoxide-iodic acid hybrid clusters, the sorption of water vapor is of particular interest, as water facilitates the

1
2
3 interconversion of iodine pentoxide and iodic acid.⁴¹⁻⁴² We examined water vapor sorption at 295
4 K and saturation ratios from 0.0 to 0.65 through monitoring CCS shifts for the cluster ions
5
6 $(\text{HIO}_3)\text{IO}_3^-$ and $(\text{I}_2\text{O}_5)_x\text{IO}_3^-$ ($x = 1 - 7$). Figure 3a displays plot of the CCS as a function of
7
8 saturation ratio. It is evident in the figure that CCSs for all cluster ions measured increase
9
10 noticeably, but by less than 12% over the saturation ratio range examined. This is a clear
11
12 indication of water vapor sorption, but not to the extent wherein cluster ions would sorb
13
14 sufficient quantities of water to behave as nanometer scale droplets (i.e. where clusters, by
15
16 volume, are largely composed of condensing solvent, as has been observed for cluster ions
17
18 exposed to some organic species).⁴³ We can additionally compare the extent of observed CCS
19
20 shifts to the computed change in CCS associated with the sorption of water vapor molecules.
21
22 Figure 3b displays plot of the ratio $\text{CCS}_g/\text{CCS}_0$, where CCS_g is the DHSS computed collision
23
24 cross section in CO_2 for a cluster ion with g water molecules attached to it. Details on cluster ion
25
26 structure modeling are again provided in the *Supporting Information*. For the ions $(\text{HIO}_3)\text{IO}_3^-$
27
28 and $(\text{I}_2\text{O}_5)_x\text{IO}_3^-$ ($x = 1 - 3$), $\text{CCS}_g/\text{CCS}_0$ and $\text{CCS}_g/\text{CCS}_0$ fall in similar ranges for $g = 5$ and
29
30 smaller (where CCS_5 is the collision cross section inferred from measurement at saturation ratio
31
32 S), and for $(\text{I}_2\text{O}_5)_4\text{IO}_3^-$ for $g = 10$ and smaller. This suggests that water vapor sorption does occur
33
34 to a sufficient extent to complete the reaction $\text{I}_2\text{O}_5 + \text{H}_2\text{O} \rightarrow 2\text{HIO}_3$ for realistic relative humidity
35
36 levels, but water vapor sorption beyond the level required for iodic acid formation is limited to
37
38 only a few water molecules (i.e. fewer than 20 water molecules). We further remark that despite
39
40 the apparent sorption of water vapor during mobility measurement, passage through the high
41
42 pressure drop mass spectrometer inlet or through the quadrupoles appears to lead to complete
43
44 loss of excess water. Ions are thus still detected at the mass channel for dehydrated $(\text{I}_2\text{O}_5)_x\text{IO}_3^-$.
45
46
47
48
49
50
51
52
53
54
55
56
57
58
59
60

Additional quantitative information on the extent of water vapor binding can be gained by comparing observed CCS_S/CCS_0 ratios to a Langmuir-like sorption model:^{20, 40, 43}

$$\frac{CCS_S}{CCS_0} = \left[\sum_{g=0}^{\zeta} \left(\frac{P_g}{\left(1 + S \frac{M_{H_2O}^{n_{sat}}}{M_{CO_2}^{n_{CO_2}}}\right)^{-1} \frac{CCS_{g,CO_2}}{CCS_0} + \left(1 + \frac{1}{S} \frac{M_{CO_2}^{n_{CO_2}}}{M_{H_2O}^{n_{sat}}}\right)^{-1} \left(\frac{M_{CO_2}}{M_{H_2O}}\right)^{1/2} \frac{CCS_{g,H_2O}}{CCS_0}} \right) \right]^{-1} \quad (1)$$

$$P_g = \frac{S^g \prod_{j=1}^g \left(\frac{\zeta+1}{j} - 1\right)}{1 + \sum_{m=1}^{\zeta} S^m \prod_{j=1}^m \left(\frac{\zeta+1}{j} - 1\right)} \quad g \geq 1 \quad (2)$$

$$P_0 = \frac{1}{1 + \sum_{m=1}^{\zeta} S^m \prod_{j=1}^m \left(\frac{\zeta+1}{j} - 1\right)} \quad (3)$$

In Equations (1-3), P_g is the probability that a cluster has g water vapor molecules sorbed, M_{H_2O} and M_{CO_2} are the molecular masses of water and carbon dioxide, respectively, n_{sat} is the water vapor number concentration at saturation, n_{CO_2} is the carbon dioxide number concentration at atmospheric pressure, CCS_{g,CO_2} is the computed CCS of a cluster with g water molecules bound in CO_2 bath gas, and CCS_{g,H_2O} is the computed CCS of a cluster with g water molecules bound in H_2O bath gas. ζ is a fitting parameter representing the maximum number of water vapor molecules which can bind to the cluster ion. The equation (1) calculated average collision cross section (CCS_S) is required for comparison between model and experiments because the number of water molecules sorbed to a cluster during measurement is not constant; molecules constantly sorb and desorb from a cluster ion. A more complete derivation of these equations is provided in the *Supporting Information*. Figure 3c displays comparison of the Langmuir model predictions to experimental measurements for selected cluster ions, using fit values of ζ . Results show that the Langmuir model best fits experimental results when ζ exceeds the required number of water vapor molecules needed for completion of the reaction $I_2O_5 + H_2O \rightarrow 2HIO_3$ by 7-14 water molecules. Thus, the modeling approach confirms that iodic acid clusters are only mildly

hydrated under atmospherically relevant conditions, and not hydrated to a level where ion-pairs would wholly or partially dissociate and the clusters would be described as nanodroplets.

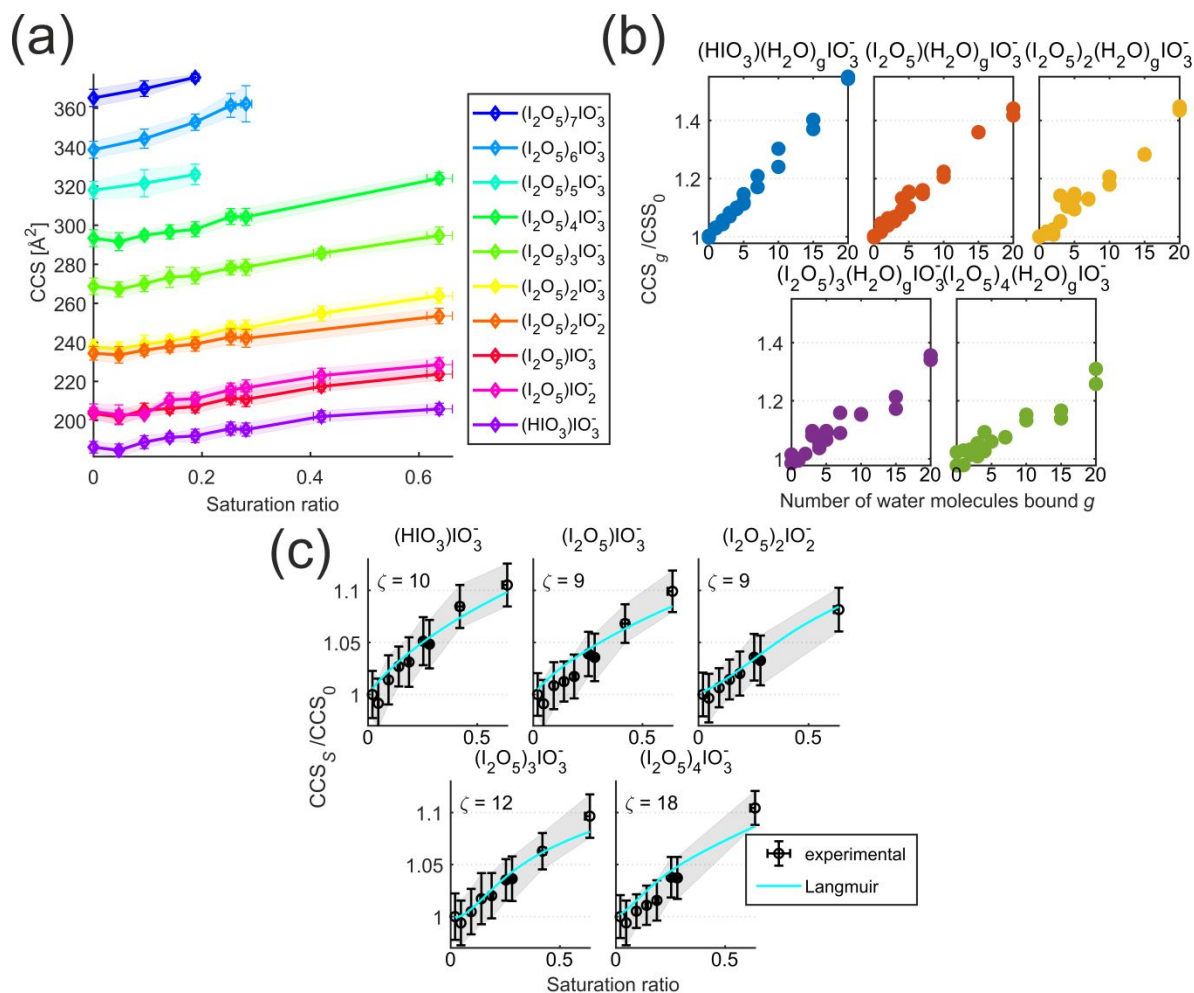


Figure 3. (a) The measured CCS as a function of saturation ratio. (b) The computed ratio CCS_g/CCS_0 as function of the number of water molecules (g) bound to a cluster ion. (c) A comparison of the CCS given by the Langmuir-model fitted to experimental data for 5 selected cluster ions. The value of the fitting parameter ζ , the maximum number of water molecules which can bind to each cluster, is noted. Error bars are based upon the uncertainty in the mobility analyzer voltage corresponding to the peak signal intensity.

In total, our results provide insight into the properties of iodine pentoxide-iodic acid hybrid clusters, similar in chemical composition to those formed in atmospheric nucleation events in coastal regions. IM-MS measurements suggest that such clusters are highly stable and at atmospherically relevant relative humidities, they can sorb sufficient quantities of water for

1
2
3 conversion of most iodine pentoxide to iodic acid. However, sorption of water vapor beyond this
4
5 level does not appear to be substantial. Combined with similar findings for dimethylamine-
6
7 sulfuric acid clusters,²¹ we suggest that in many circumstances the clusters involved in
8
9 atmospheric nucleation are only mildly hydrated, and hence further growth of such clusters
10
11 hinges upon the interaction between these clusters and the subsequently condensing species (e.g.
12
13 oxidized organic species). Comparison of measurement inferred CCSs suggest that available
14
15 computational methods yield structures which capture global structural features of clusters, as
16
17 modeled and measured CCSs are in good agreement. We suggest that further laboratory scale
18
19 experiments (e.g. infrared spectroscopy)⁴⁴ would be important to probe iodine pentoxide-iodic
20
21 acid clusters in an effort to develop models describing nucleation events driven by iodine
22
23 species.
24
25
26
27
28
29
30

31 SUPPORTING INFORMATION

32
33
34
35 Descriptions of differential mobility analyzer-mass spectrometer measurements, the
36
37 computational approaches used in cluster generation, and IMoS input parameters for collision
38
39 cross section calculations, as well as derivation of equations (1-3) are available online. Cluster
40
41 structure coordinates are additionally provided (xyz_files.zip).
42
43
44

45 AUTHOR INFORMATION

46
47 The authors declare no competing financial interests.
48
49

50 ACKNOWLEDGMENT

51
52
53 This work was supported by European Research Council project 692891-DAMOCLES, the
54
55 Academy of Finland Center of Excellence, ATMATH project and CSC – Finnish IT Centre
56
57
58
59
60

REFERENCES

- (1) Sipilä, M.; *et al.* The Role of Sulfuric Acid in Atmospheric Nucleation. *Science* **2010**, *327*, 1243-1246.
- (2) Zhang, R.; Khalizov, A.; Wang, L.; Hu, M.; Xu, W. Nucleation and Growth of Nanoparticles in the Atmosphere. *Chem. Rev.* **2012**, *112*, 1957-2011.
- (3) Weber, R. J.; Marti, J. J.; McMurry, P. H.; Eisele, F. L.; Tanner, D. J.; Jefferson, A. Measured Atmospheric New Particle Formation Rates: Implications for Nucleation Mechanisms. *Chem. Eng. Comm.* **1996**, *151*, 53-64.
- (4) Dunne, E. M.; *et al.* Global Atmospheric Particle Formation from CERN CLOUD Measurements. *Science* **2016**, *354* (6316), 1119-1124.
- (5) Almeida, J.; *et al.* Molecular Understanding of Sulphuric Acid–Amine Particle Nucleation in the Atmosphere. *Nature* **2013**, 359-363.
- (6) Kulmala, M.; *et al.* Direct Observations of Atmospheric Aerosol Nucleation. *Science* **2013**, *339*, 943-946.
- (7) Kürten, A.; *et al.* Neutral Molecular Cluster Formation of Sulfuric Acid–Dimethylamine Observed in Real Time Under Atmospheric Conditions. *Proc. Natl. Acad. Sci. U. S. A.* **2014**, *111*, 15019-15024.
- (8) Myllyls, N.; Elm, J.; Halonen, R.; Kurtén, T.; Vehkamäki, H. Coupled Cluster Evaluation of the Stability of Atmospheric Acid–Base Clusters with up to 10 Molecules. *J. Phys. Chem. A* **2016**, *120*, 621-630.
- (9) Elm, J.; Passananti, M.; Kurtén, T.; Vehkamäki, H. Diamines Can Initiate New Particle Formation in the Atmosphere. *J. Phys. Chem. A* **2017**, *121*, 6155-6164.
- (10) Glasoe, W. A.; Volz, K.; Panta, B.; Freshour, N.; Bachman, R.; Hanson, D. R.; McMurry, P. H.; Jen, C. Sulfuric Acid Nucleation: An Experimental Study of the Effect of Seven Bases. *J. Geophys. Res.: Atmos.* **2015**, *120*, 1933-1950.
- (11) Kulmala, M.; Petäjä, T.; Ehn, M.; Thornton, J.; Sipilä, M.; Worsnop, D. R.; Kerminen, V. M. Chemistry of Atmospheric Nucleation: On the Recent Advances on Precursor Characterization and Atmospheric Cluster Composition in Connection with Atmospheric New Particle Formation. *Annu. Rev. Phys. Chem.* **2014**, *65*, 21-37.
- (12) O'Dowd, C. D.; Jimenez, J. L.; Bahreini, R.; Flagan, R. C.; Seinfeld, J. H.; Hämeri, K.; Pirjola, L.; Kulmala, M.; Jennings, S. G.; Hoffmann, T. Marine Aerosol Formation from Biogenic Iodine Emissions. *Nature* **2002**, *417*, 632-636.
- (13) O'Dowd, C. D.; Hoffmann, T. Coastal New Particle Formation: A Review of the Current State-of-the-Art. *Environ. Chem.* **2006**, *2*, 245-255.

- 1
2
3 (14) Saiz-Lopez, A.; Plane, J. M. C. Novel Iodine Chemistry in the Marine Boundary Layer. *Geophys. Res. Lett.* **2004**, *31*, L04112.
4
5
6 (15) McFiggans, G.; *et al.* Iodine-Mediated Coastal Particle Formation: An Overview of the
7 Reactive Halogens in the Marine Boundary Layer (RHAMBLe) Roscoff Coastal Study.
8 *Atmos. Chem. Phys.* **2010**, *10*, 2975-2999.
9
10 (16) Hoffmann, T.; O'Dowd, C. D.; Seinfeld, J. H. Iodine Oxide Homogeneous Nucleation: An
11 Explanation for Coastal New Particle Production. *Geophys. Res. Lett.* **2001**, *28*, 1949-1952.
12
13 (17) Sipilä, M.; *et al.* Molecular-Scale Evidence of Aerosol Particle Formation via Sequential
14 Addition of HIO₃. *Nature* **2016**, *537*, 532-534.
15
16 (18) Lanucara, F.; Holman, S. W.; Gray, C. J.; Evers, C. E. The Power of Ion Mobility-Mass
17 Spectrometry for Structural Characterization and the Study of Conformational Dynamics.
18 *Nat. Chem.* **2014**, *6*, 281-294.
19
20 (19) Hogan, C. J.; Fernandez de la Mora, J. Tandem Ion Mobility-Mass Spectrometry (IMS-
21 MS) Study of Ion Evaporation from Ionic Liquid-Acetonitrile Nanodrops. *Phys. Chem.*
22 *Chem. Phys.* **2009**, *11*, 8079-8090.
23
24 (20) Oberreit, D.; Rawat, V. K.; Larriba-Andaluz, C.; Ouyang, H.; McMurry, P. H.; Hogan, C.
25 J. Analysis of Heterogeneous Water Vapor Uptake by Metal Iodide Cluster Ions via
26 Differential Mobility Analysis-Mass Spectrometry. *J. Chem. Phys.* **2015**, *143*, 104204.
27
28 (21) Thomas, J. M.; He, S.; Larriba-Andaluz, C.; DePalma, J. W.; Johnston, M. V.; Hogan, C. J.
29 Ion Mobility Spectrometry-Mass Spectrometry Examination of the Structures, Stabilities,
30 and Extents of Hydration of Dimethylamine-Sulfuric Acid Clusters. *Phys. Chem. Chem.*
31 *Phys.* **2016**, *18*, 22962-22972.
32
33 (22) Larriba, C.; Hogan, C. J. Ion Mobilities in Diatomic Gases: Measurement versus Prediction
34 with Non-Specular Scattering Models. *J. Phys. Chem. A* **2013**, *117*, 3887-3901.
35
36 (23) Shrivastav, V.; Nahin, M.; Hogan, C. J.; Larriba-Andaluz, C. Benchmark Comparison for a
37 Multi-Processing Ion Mobility Calculator in the Free Molecular Regime. *J. Am. Soc. Mass*
38 *Spectrom.* **2017**, *28*, 1540-1551.
39
40 (24) Ude, S.; Fernandez de la Mora, J. Molecular Monodisperse Mobility and Mass Standards
41 from Electrosprays of Tetra-Alkyl Ammonium Halides. *J. Aerosol Sci.* **2005**, *36*, 1224-
42 1237.
43
44 (25) Valerie, G.; *et al.* Recommendations for Reporting Ion Mobility Mass Spectrometry
45 Measurements. *Mass Spectrometry Reviews* **2018**, In Press. DOI: 10.1002/mas.21585
46
47 (26) Hogan, C. J.; Fernandez de la Mora, J. Ion-Pair Evaporation from Ionic Liquid Clusters. *J.*
48 *Am. Soc. Mass Spectrom.* **2010**, *21*, 1382-1386.
49
50
51
52
53
54
55
56
57
58
59
60

- 1
2
3 (27) Ouyang, H.; Larriba-Andaluz, C.; Oberreit, D. R.; Hogan, C. J. The Collision Cross
4 Sections of Iodide Salt Cluster Ions in Air via Differential Mobility Analysis-Mass
5 Spectrometry. *J. Am. Soc. Mass Spectrom.* **2013**, *24*, 1833-1847.
6
7
8 (28) Marti, J. J.; Weber, R. J.; McMurry, P. H.; Eisele, F.; Tanner, D.; Jefferson, A. New
9 Particle Formation at a Remote Continental Site: Assessing the Contributions of SO₂ and
10 Organic Precursors. *J. Geophys. Res.: Atmos.* **1997**, *102*, 6331-6339.
11
12 (29) DePalma, J. W.; Bzdek, B. R.; Doren, D. J.; Johnston, M. V. Structure and Energetics of
13 Nanometer Size Clusters of Sulfuric Acid with Ammonia and Dimethylamine. *J. Phys.*
14 *Chem. A* **2012**, *116*, 1030-1040.
15
16 (30) Chen, M.; *et al.* Acid-Base Chemical Reaction Model for Nucleation Rates in the Polluted
17 Atmospheric Boundary Layer. *Proc. Natl. Acad. Sci. U. S. A.* **2012**, *109*, 18713-18718.
18
19 (31) McMurry, P. H.; Li, C. The Dynamic Behavior of Nucleating Aerosols in Constant
20 Reaction Rate Systems: Dimensional Analysis and Generic Numerical Solutions. *Aerosol*
21 *Sci. Tech.* **2017**, *51*, 1057-1070.
22
23 (32) Mason, E. A.; McDaniel, E. W. *Transport Properties of Ions in Gases*. Wiley: New York,
24 1988.
25
26 (33) Zhang, J.; Dolg, M. ABCluster: the artificial bee colony algorithm for cluster global
27 optimization. *Phys. Chem. Chem. Phys.* **2015**, *17*, 24173-24181.
28
29 (34) Larriba, C.; Hogan, C. J. Free Molecular Collision Cross Section Calculation Methods for
30 Nanoparticles and Complex Ions with Energy Accommodation. *J. Comput. Phys.* **2013**,
31 *251*, 344-363.
32
33 (35) Fernández-García, J.; Fernández de la Mora, J. Electrical Mobilities of Multiply Charged
34 Ionic-Liquid Nanodrops in Air and Carbon Dioxide Over a Wide Temperature Range:
35 Influence of Ion-Induced Dipole Interactions. *Phys. Chem. Chem. Phys.* **2014**, *16*, 20500-
36 20513.
37
38 (36) Larriba-Andaluz, C.; Fernandez-Garcia, J.; Ewing, M. A.; Hogan, C. J.; Clemmer, D. E.
39 Gas Molecule Scattering & Ion Mobility Measurements for Organic Macro-Ions in He
40 Versus N₂ Environments. *Phys. Chem. Chem. Phys.* **2015**, *17*, 15019-15029.
41
42 (37) Maißer, A.; Thomas, J. M.; Larriba-Andaluz, C.; He, S.; Hogan Jr, C. J. The Mass-
43 Mobility Distributions of Ions Produced by a Po-210 source in Air. *J. Aerosol Sci.* **2015**,
44 *90*, 36-50.
45
46 (38) Pepin, R.; Petrone, A.; Laszlo, K. J.; Bush, M. F.; Li, X.; Tureček, F. Does Thermal
47 Breathing Affect Collision Cross Sections of Gas-Phase Peptide Ions? An Ab Initio
48 Molecular Dynamics Study. *J. Phys. Chem. Lett.* **2016**, *7*, 2765-2771.
49
50
51
52
53
54
55
56
57
58
59
60

- 1
2
3 (39) Kwantwi-Barima, P.; Ouyang, H.; Hogan, C. J.; Clowers, B. H. Tuning Mobility
4 Separation Factors of Chemical Warfare Agent Degradation Products via Selective Ion-
5 Neutral Clustering. *Anal. Chem.* **2017**, *89*, 12416-12424.
6
7 (40) Rawat, V. K.; Vidal-de-Miguel, G.; Hogan, C. J. Modeling Vapor Uptake Induced
8 Mobility Shifts in Peptide Ions Observed with Transversal Modulation Ion Mobility
9 Spectrometry-Mass Spectrometry. *Analyst* **2015**, *140*, 6945-6954.
10
11 (41) Murray, B. J.; *et al.* Glass Formation and Unusual Hygroscopic Growth of Iodic Acid
12 Solution Droplets with Relevance for Iodine Mediated Particle Formation in the Marine
13 Boundary Layer. *Atmos. Chem. Phys.* **2012**, *12*, 8575-8587.
14
15 (42) Smith, D. K.; Pantoya, M. L.; Parkey, J. S.; Kesmez, M. The Water-Iodine Oxide System:
16 A Revised Mechanism for Hydration and Dehydration. *RSC Advances* **2017**, *7*, 10183-
17 10191.
18
19 (43) Li, C.; Hogan, C. J. Vapor Specific Extents of Uptake by Nanometer Scale Charged
20 Particles. *Aerosol Sci. Tech.* **2017**, *51*, 653-664.
21
22 (44) Waller, S. E.; Yang, Y.; Castracane, E.; Racow, E. E.; Kreinbihl, J. J.; Nickson, K. A.;
23 Johnson, C. J. The Interplay Between Hydrogen Bonding and Coulombic Forces in
24 Determining the Structure of Sulfuric Acid-Amine Clusters. *J. Phys. Chem. Lett.* **2018**, *9*,
25 1216-1222.
26
27
28
29
30
31
32
33
34
35
36
37
38
39
40
41
42
43
44
45
46
47
48
49
50
51
52
53
54
55
56
57
58
59
60

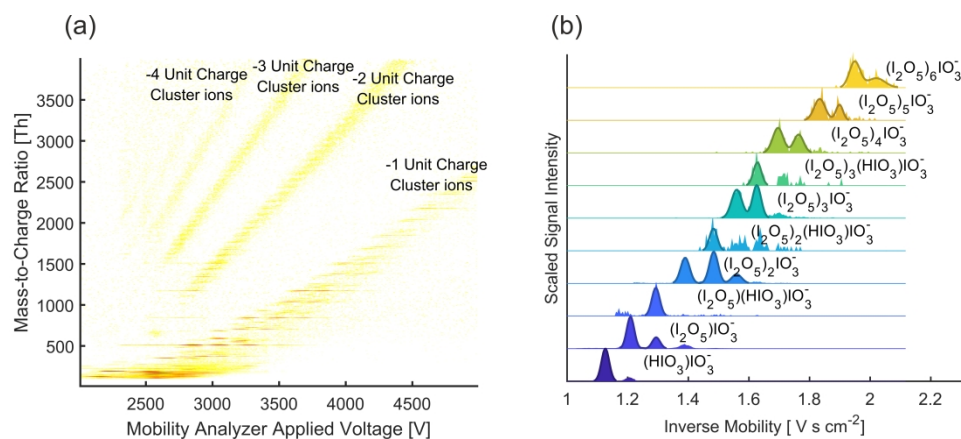


Figure 1. (a) A contour plot of measured signal intensity as a function of mass-to-charge ratio and mobility analyzer applied voltage for electrospray generated cluster anions. (b) Post-calibration inverse mobility spectra for specific mass identified cluster anions. The chemical compositions of the selected ions are noted.

270x114mm (600 x 600 DPI)

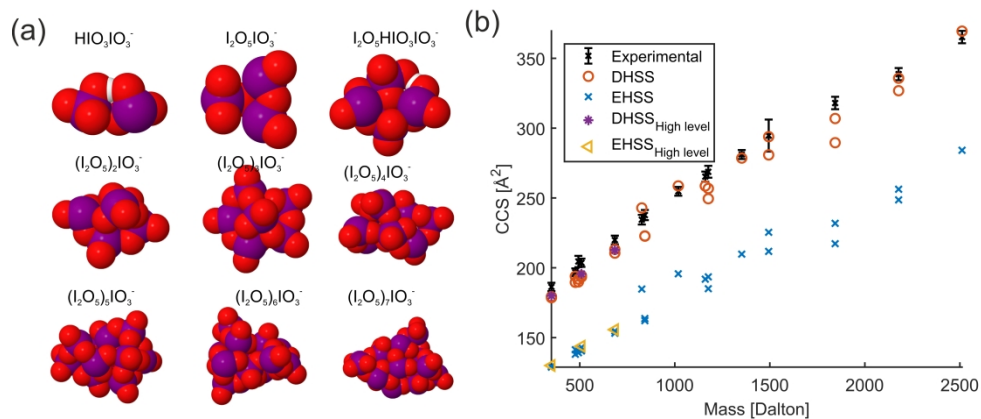


Figure 2. (a) Depictions of selected cluster ion candidate structures. Purple: Iodine atoms. Red: Oxygen atoms. (b) Experimentally inferred and calculated CCSs as a function of cluster ion mass. The subscript "High Level" refers to structures obtained from density function theory ($\omega\text{B97xD//aug-cc-pVTZ-PP}$ level) using a sufficiently large basis set. Error bars are based upon the uncertainty in the mobility analyzer voltage corresponding to the peak signal intensity.

264x111mm (600 x 600 DPI)

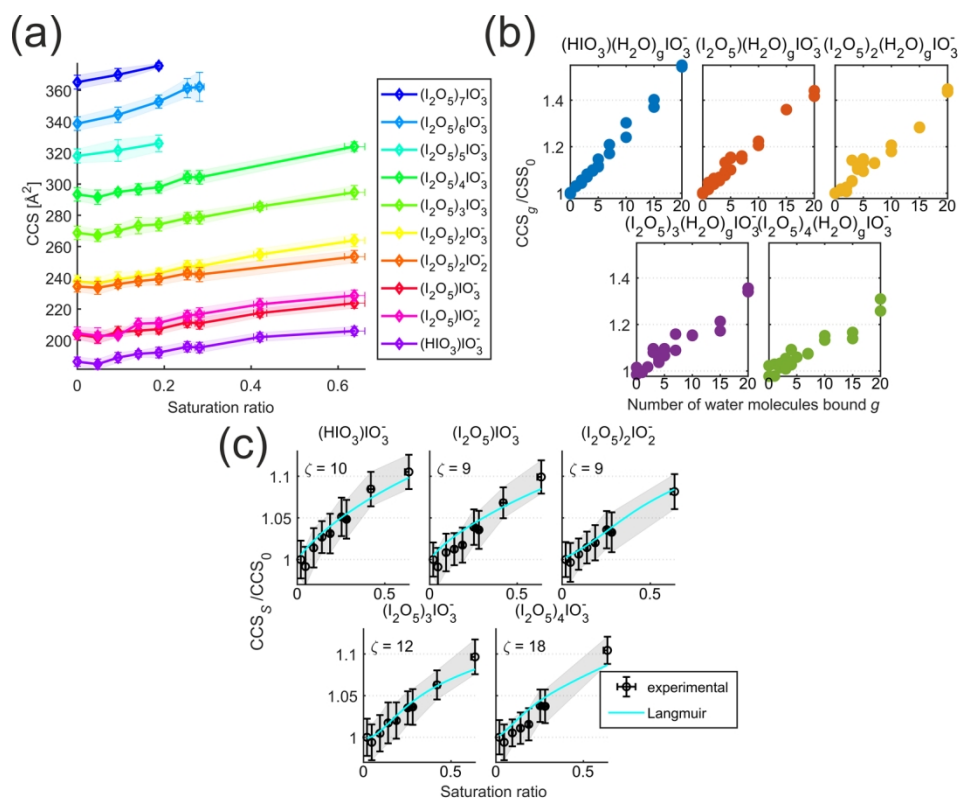


Figure 3. (a) The measured CCS as a function of saturation ratio. (b) The computed ratio CCS_g/CCS_0 as function of the number of water molecules (g) bound to a cluster ion. (c) A comparison of the CCS given by the Langmuir-model fitted to experimental data for 5 selected cluster ions. The value of the fitting parameter ζ , the maximum number of water molecules which can bind to each cluster, is noted. Error bars are based upon the uncertainty in the mobility analyzer voltage corresponding to the peak signal intensity.

291x230mm (150 x 150 DPI)